Author/s:
Lindegaard, B;Matthews, VB;Brandt, C;Hojman, P;Allen, TL;Estevez, E;Watt, MJ;Bruce, CR;Mortensen, OH;Syberg, S;Rudnicka, C;Abildgaard, J;Pilegaard, H;Hidalgo, J;Ditlevsen, S;Alsted, TJ;Madsen, AN;Pedersen, BK;Febbraio, MA

Title:
Interleukin-18 activates skeletal muscle AMPK and reduces weight gain and insulin resistance in mice

Date:
2013-09-01

Citation:
Lindegaard, B., Matthews, V. B., Brandt, C., Hojman, P., Allen, T. L., Estevez, E., Watt, M. J., Bruce, C. R., Mortensen, O. H., Syberg, S., Rudnicka, C., Abildgaard, J., Pilegaard, H., Hidalgo, J., Ditlevsen, S., Alsted, T. J., Madsen, A. N., Pedersen, B. K. & Febbraio, M. A. (2013). Interleukin-18 activates skeletal muscle AMPK and reduces weight gain and insulin resistance in mice. Diabetes, 62 (9), pp.3064-3074. https://doi.org/10.2337/db12-1095.

Persistent Link:
https://hdl.handle.net/11343/255743

Interleukin-18 Activates Skeletal Muscle AMPK and Reduces Weight Gain and Insulin Resistance in Mice

Birgitte Lindegaard,[1,2,7] Vance B. Matthews,[7,8] Claus Brandt,[1,2] Pernille Hojman,[1,2] Tamara L. Allen,[7] Emma Estevez,[7] Matthew J. Watt,[9] Clinton R. Bruce,[7,9] Ole H. Mortensen,[1,2] Susanne Syberg,[1,10] Caroline Rudnicka,[8] Julie Abildgaard,[1] Henriette Pilegaard,[1,3] Juan Hidalgo,[11] Susanne Ditlevsen,[4] Thomas J. Alsted,[5] Andreas N. Madsen,[6] Bente K. Pedersen,[1,2] and Mark A. Febbraio[7]

Circulating interleukin (IL)-18 is elevated in obesity, but paradoxically causes hypophagia. We hypothesized that IL-18 may attenuate high-fat diet (HFD)-induced insulin resistance by activating AMP-activated protein kinase (AMPK). We studied mice with a global deletion of the α-isoform of the IL-18 receptor ($IL\text{-}18R^{-/-}$) fed a standard chow or HFD. We next performed gain-of-function experiments in skeletal muscle, in vitro, ex vivo, and in vivo. We show that IL-18 is implicated in metabolic homeostasis, inflammation, and insulin resistance via mechanisms involving the activation of AMPK in skeletal muscle. $IL\text{-}18R^{-/-}$ mice display increased weight gain, ectopic lipid deposition, inflammation, and reduced AMPK signaling in skeletal muscle. Treating myotubes or skeletal muscle strips with IL-18 activated AMPK and increased fat oxidation. Moreover, in vivo electroporation of IL-18 into skeletal muscle activated AMPK and concomitantly inhibited HFD-induced weight gain. In summary, IL-18 enhances AMPK signaling and lipid oxidation in skeletal muscle implicating IL-18 in metabolic homeostasis. ***Diabetes* 62:3064–3074, 2013**

The cytokine interleukin (IL)-18 was identified ~15 years ago as a cofactor that, together with IL-12, stimulates production of interferon-γ (1). This ~18-kDa cytokine, which has structural similarities to the IL-1 cytokine family, is widely expressed in many mammalian cells and tissues, including liver, adipose tissue, skeletal muscle, pancreas, brain, and endothelium (2). IL-18 is best known for its role in inflammation, whereby proinflammatory stimuli such as lipopolysaccharide, Fas ligand, and tumor necrosis factor-α lead to caspase-1–mediated cleavage of pro-IL-18 into mature IL-18. IL-18 then can signal via a heterodimer of the transmembrane IL-18 receptors (α and β) and via a Toll-like receptor signaling cascade, ultimately leading to the activation of nuclear factor-κB and subsequent regulation of gene transcription (3). Although this is the most characterized signaling pathway for this cytokine, it is worth noting that IL-18 also has been implicated in mitogen-activated protein kinase, phosphatidylinositol 3-kinase, and signal transducer and activator of transcription (STAT) 3 signaling (4), which are all implicated in energy metabolism.

It is now well-accepted that obesity results in a state of low-grade chronic inflammation (5); therefore, it is not surprising that circulating IL-18 levels are elevated in human obesity (6) and in patients with type 2 diabetes (7). Somewhat paradoxically, the works of two separate groups have reported that mice with a global deletion of IL-18 become obese and insulin-resistant, whereas exogenous administration of recombinant IL-18 rescued this phenotype (8,9). These previous studies ascribed the mechanism of action of IL-18 in modulating nutrient homeostasis to be exclusively via neuronal control of food intake (8,9). However, in the earlier study (8), the authors demonstrated that the $IL\text{-}18^{-/-}$ mice displayed decreased peripheral insulin sensitivity and that IL-18 signals via STAT3 in the liver, increasing the possibility that IL-18 may play a role in peripheral energy metabolism because STAT3 plays a major role in maintaining metabolic homeostasis in the liver (10). In addition, we (11,12) and others (13,14) have shown that cytokines that result in activation of STAT3 via transmembrane receptor signaling can activate the AMP-activated kinase (AMPK) signaling pathway to enhance fat oxidation in skeletal muscle, thereby attenuating high-fat diet (HFD)-induced insulin resistance. Together, these previous studies increase the possibility that IL-18 may attenuate HFD-induced insulin resistance via affecting metabolic processes, such as activation of AMPK, in skeletal muscle. This is important from a therapeutic viewpoint because drugs that effectively modulate food intake via targeting the central nervous system have, to date, proven unsuccessful because of side effects associated with activation of the lateral hypothalamus (15). In the current study, we tested the hypothesis that IL-18 signaling can modulate nutrient homeostasis via mechanisms associated with peripheral energy metabolism. We show that IL-18 activates AMPK and increases lipid oxidation in skeletal muscle, implicating IL-18 in diet-induced obesity and insulin resistance.

RESEARCH DESIGN AND METHODS

Animal experimental protocols. For the diet intervention study, 12-week-old *Il18R*$^{-/-}$ (back-crossed 11 generations to C57BL/6J) and wild-type C57BL/6J mice were obtained from Charles River Laboratories (L'Arbresle, France).

From the [1]Centre of Inflammation and Metabolism, Rigshospitalet, Copenhagen, Denmark; the [2]Department of Infectious Diseases, University of Copenhagen, Copenhagen, Denmark; the [3]Department of Biology, University of Copenhagen, Copenhagen, Denmark; the [4]Department of Mathematical Sciences, University of Copenhagen, Copenhagen, Denmark; the [5]Department of Physiology, University of Copenhagen, Copenhagen, Denmark; the [6]Department of Molecular Pharmacology, University of Copenhagen, Copenhagen, Denmark; the [7]Cellular and Molecular Metabolism Laboratory, Baker IDI Heart and Diabetes Institute, Melbourne, Australia; the [8]University of Western Australia Centre for Medical Research, Western Australian Institute for Medical Research, Perth, Australia; the [9]Department of Physiology, Monash University, Clayton, Australia; the [10]Osteoporosis Unit, Hvidovre Hospital, Hvidovre, Denmark; and the [11]Institute of Neurosciences, Department of Cellular Biology, Physiology, and Immunology, Animal Physiology Unit, Faculty of Sciences, Autonomous University of Barcelona, Barcelona, Spain.

Corresponding author: Mark A. Febbraio, mark.febbraio@bakeridi.edu.au, or Bente K. Pedersen, bente.klarlund.pedersen@rh.regionh.dk.

Received 14 August 2012 and accepted 7 May 2013.

DOI: 10.2337/db12-1095

This article contains Supplementary Data online at http://diabetes.diabetesjournals.org/lookup/suppl/doi:10.2337/db12-1095/-/DC1.

Subsequent to this initial cohort, we then performed experiments in *Il18R*$^{-/-}$ and wild-type mice obtained from heterozygous mating. Eight-week-old C57BL/6J mice (inbred; Herlev, Denmark) were used for a DNA electroporation study, and 13-week-old C57/BL6 mice (inbred; Melbourne, Australia) were used for ex vivo experiments. All experiments were approved by The Animal Experiments Inspectorate in Denmark or the Baker IDI Alfred Medical Research and Education Precinct Animal Ethics Committee (or both) in accordance with the National Health and Medical Research Council of Australia Guidelines on Animal Experimentation. Mice were maintained on a 12-h light, 12-h dark cycle on a standard rodent chow diet (27%, 13%, and 60% kcal from protein, fat, and carbohydrates, respectively) or HFD composed of 60% calories from fat (Research Diets 12492; 20%, 60%, and 20% kcal from protein, fat, and carbohydrates, respectively) for 18 weeks (diet-induced obesity study) or 4 weeks (in vivo electroporation study).

In vivo electroporation experiments were performed as previously described (16). Briefly, the regulatory plasmid pTet-On was obtained from Clontech (Palo Alto, CA). Because IL-18 lacks a typical signal sequence, the V-J2-C region of murine immunoglobin k-chain was cloned upstream of the mature IL-18 sequence. The tibialis anterior muscle of each mouse was directly injected with 20 μL plasmid solution (0.5 μg/μL) and electric pulsing was applied using 4-mm plate electrodes and an electric field of one high-voltage pulse (100 μs, 800 V/cm) and one low-voltage pulse (400 ms, 100 V/cm) (17). Induction of gene expression was obtained by administering drinking water consisting of distilled water containing 0.2 mg/mL doxycycline (doxycycline hyclate; Sigma-Aldrich) (18).

For ex vivo experiments, mice were fed a standard chow diet and drinking water, available ad libitum. To examine palmitate metabolism, mice were first anesthetized and soleus muscles were carefully dissected into longitudinal strips from tendon to tendon. Strips were removed and [^{14}C]palmitate oxidation was analyzed as previously described (19). The dose of 100 ng/mL IL-18 was used and PBS served as placebo. The strips from the same animal were used for both IL-18 and PBS.

Skeletal muscle cell culture. To examine whether IL-18 affected phosphorylation (Thr^{172}) of AMPK and acetyl CoA carboxylase-β (ACCβ; Ser^{79}), fully fused L6 myotubes were treated with recombinant rat IL-18 (MBL, Woburn, MA). Cells were treated with IL-18 for 10, 30, and 60 min at doses of 1 and 10 ng/mL.

Analysis of body composition. We measured body composition analysis in IL18R$^{-/-}$ by dual-energy X-ray absorptiometry using the Lunar PIXImus Mouse Densitometer (GE Medical Systems) and in IL-18 electroporated mice by using a Lunar Prodigy scanner with a small animal software application (GE Healthcare Systems). Animals were anesthetized by intraperitoneal injection of Hypnorm (0.4 mL/kg; Janssen, Saunderton, U.K.) and Dormicum (2 mg/kg; Roche, Basel, Switzerland), and laid flat on the scanning platform on their ventral side. To confirm dual-energy X-ray absorptiometry fat mass determination, mice were killed and two intra-abdominal fat pads (gonadal, retroperitoneal) and one subcutaneous fat pad (inguinal) were dissected and weighed.

Insulin tolerance tests. We performed insulin tolerance tests in 7.5-month-old male mice 4 h after removal of food. Blood samples were obtained by tail cut and were analyzed for glucose content using a glucometer (Accu-chek Compact plus) immediately before and at 15, 30, 45, 60, 90, and 120 min after an intraperitoneal injection of insulin (0.75 units/kg; Actrapid; Novo Nordisk).

Indirect calorimetry. Mice were placed in a 16-chamber indirect calorimetry system (TSE Systems, Bad Homburg, Germany) cages for 10 days; the first 5 days were considered the acclimation phase and data were analyzed only for the last final days. After 3 days, the mice were fasted for 24 h. The Vo_2 (mL/h/kg), respiratory exchange ratio, and activity (beam breaks) were measured using the system. Mice had free access to food and water while in the chambers. Food intake was measured for the duration of data collection while mice underwent the indirect calorimetry measurements.

Plasma parameters analysis. We collected blood samples from the tail vein of the mice into EDTA tubes and they were immediately spun at 6,000*g* for 10 min at 4°C and plasma was removed. Plasma was stored at −80°C until analysis. Plasma insulin was determined by ELISA (Crystal Chem). Blood glucose was measured by glucometer (Accu-chek Compact Plus). Adiponectin concentration was measured by RIA kit. Leptin, monocyte chemoattractant protein 1, plasminogen activator inhibitor 1, IL-6, and tumor necrosis factor-α were measured by using a Lincoplex mouse serum adipokine panel (Linco).

Insulin signaling tissue collection. Animals were anesthetized with an injection of Hypnorm (0.4 mL/kg; Janssen, Saunderton, UK) and Dormicum (2 mg/kg; Roche, Basel, Switzerland), and the gastrocnemius muscle as well as the right lobe of the liver (after a ligature around the blood vessel) were removed and stored in liquid nitrogen until further processing. This was followed by injection of insulin (1.5 units/kg lean body mass) into the abdominal aorta and removal of the contralateral gastrocnemius and liver lobe occurred 2 min after injection. Samples were stored in liquid nitrogen until further processing.

RNA extraction and real-time quantitative PCR. Mouse tissue was isolated, frozen in liquid nitrogen or in dry ice and absolute alcohol, and stored at −80°C until extraction. Total RNA was isolated from adipose tissue with TriZol (Life Technology), as described by the manufacturer; 500 ng RNA was reverse-transcribed to cDNA with the use of random hexamers (Taqman reverse-transcription reagents; Applied Biosystems). Real-time PCR was performed on an ABI PRISM 7900 sequence detector or 7500 fast sequence detector (Applied Biosystems). Each assay included (in triplicate) the following: a cDNA standard curve of five serial dilution points (range, 1–0.01); a no-template control; a no-reverse-transcriptase control; and 7.5 ng (0.375 ng for 18S rRNA) of each sample cDNA. For *18S rRNA*, *SREEBP1c*, fatty acid synthase (*FAS*), *HADB*, phosphoenolpyruvate carboxykinase (*PEPCK*), glucose-6 phosphate dehydrogenase, and carnitine palmitoyl transferase 1 (*CPT1*), the amplification mixtures were prepared with 2X Taqman Universal PCR master mix. All assay reagents were from Applied Biosystems. Primers and Taqman probes were designed for sterol regulatory–element binding protein-1c and *FAS* using a mouse-specific database (ensemble.com) and Primer Express (Applied Biosystems) and primers for *CPT1* and *HADB* were designed using the free program primer3. The sequences to amplify a fragment of sterol regulatory–element binding protein-1c was as follows: FP: 5′ GACCACGGAGCCATGGAT; 3′and RP: 5′ GGCCCGGGAAGTCACTGT; 3′ and TaqMan probe: 5′ ACATTTGAAGACATGCTCCAGCTCATCAACA; 3′, a fragment of *FAS* FP: 5′ ATCCTGGAACGAGAACACGATCT 3′; RP: 5′ GGACTTGGGGGCTGTCGTGTCA; 3′ and TaqMan probe: 5′ CACGCTGCGGAAACTTCAGGAAATGT; 3′, a fragment of *HAD* FP: GTGGAGAAGACCCTGAGCTA; RP: GCAAATCGGTCTTGTCTAGT; a fragment of *PEPCK* FP: GGCGGAGCATATGCT and RP: CCACAGGCACTAGGGAAGGC, a fragment of glucose-6 phosphate dehydrogenase FP: TCAACCTCGTCTTCAAGTGGATT; RP: GCTGTAGTAGTCGGTGTCCAGGA; CPTI FP: GTCGCTTCTTCAAGGTCTGG; and RP: AAGAAAGCAGCACGTTCCAT. Oligos for *SREBP1* and *FAS* were obtained from TaqCopenhagen (Copenhagen, Denmark) for *CPT1*, oligos for *HAD* were obtained from DNA technology (Aarhus, Denmark), and oligos for *PEPCK* and glucose-6 phosphate dehydrogenase were obtained from Geneworks (South Australia, Australia). The *18S rRNA* content was determined using a predeveloped assay reagent (Applied Biosystems). The relative concentrations of measured mRNAs were determined by plotting the threshold cycle versus the log of the serial dilution points, and the relative expression of the gene of interest was determined after normalization to *18S*, which was unaffected by genotype and diet.

AMPK activity and lipid measurements. AMPK activity was assayed in frozen tibialis anterior muscle homogenized in lysis buffer as described previously (12). Briefly, muscle lysate containing 200 μg protein was immunoprecipitated with antibody specific to the α2 or α1 catalytic subunit of AMPK and protein A/G agarose beads. Beads were washed five times, and the activity of the immobilized enzyme was assayed based on the phosphorylation of substrate for AMP-activated protein kinase peptide (0.2 mmol/L) by 0.2 mmol/L ATP (containing 2 μCi [γ-^{32}P] ATP) in the presence and absence of 0.2 mmol/L AMP. Label incorporation into the substrate for AMP-activated protein kinase peptide was measured on a Racbeta 1214 scintillation counter. For measurement of intramuscular triglycerides, freeze-dried muscle samples were dissected free of visible connective tissue and blood. Lipid was extracted by a Folch extraction, the triacylglycerol was saponified in an ethanol/KOH solution at 60°C, and glycerol content was determined fluorometrically as described previously (12).

Protein analysis. Tissue lysates (40 μg) were solubilized in Laemmli sample buffer and boiled for 5 min, resolved by SDS-PAGE on 10% polyacrylamide gels, transferred (semi-dry) to nitrocellulose membrane, blocked with 5% BSA, and immunoblotted with primary antibodies (2.5% BSA) overnight. After incubation in horseradish peroxidase-conjugated secondary antibody (2.5% BSA; Amersham Bioscience), the immunoreactive proteins were detected with enhanced chemiluminescence (Amersham Bioscience) and quantified by densitometry (ChemiDoc XRS). Membranes were stripped, washed, and reprobed for total protein content or housekeeping protein when appropriate. Total AKT was run on a separate gel and was not stripped. Samples from mice fed a chow or HFD were run on separate gels. The antibodies used for detection of total AKT and β-actin and phosphorylation of JNK1/2, AKT, AMPKα, and ACCβ were purchased from Cell Signaling. The α-tubulin antibody was obtained from Sigma Aldrich.

Statistical analysis. All analyses were performed using SAS 9.1. We performed comparison between two groups using unpaired Student *t* test and one-way ANOVA followed the Tukey post hoc test. Time-series data were analyzed with PROC MIXED. $P < 0.05$ was considered significant. When appropriate, values were logarithmically transformed to ensure normality and equal variance.

RESULTS

IL-18 receptor–deficient mice are prone to weight gain that is not associated with hyperphagia. To evaluate the role of IL-18 signaling in the etiology of body weight homeostasis, we first performed loss-of-function experiments by phenotyping mice with a global deletion of the α-isoform of the IL-18 receptor (IL-18R$^{-/-}$). Consistent with a previous study (8), IL-18R$^{-/-}$ mice become heavier than their wild-type counterparts (control [CON]) at ~6 months of age when fed a regular chow diet (Fig. 1*A*).

The increase in body mass was attributable to an increase in adiposity because we observed differences in percent fat (Fig. 1*B*) but not in percent fat-free mass (data not shown). This increase in adiposity was attributable to increases in visceral, but not subcutaneous, fat mass because both epididymal and retroperitoneal, but not inguinal, fat pad masses were higher in IL-18R$^{-/-}$ mice relative to CON (Fig. 1*C*). Although both IL-18R$^{-/-}$ and CON mice had markedly increased body mass and fat pad mass when fed an HFD for 16 weeks, the differences observed when comparing genotypes on a regular chow diet were not evident when animals were fed an HFD (Fig. 1*A–D*). As discussed, previous studies have demonstrated that IL-18$^{-/-}$ mice are prone to weight gain because of hyperphagia (8,9). Although the earlier study reported weight gain and insulin resistance in IL-18R$^{-/-}$ mice, they did not make reference to altered feeding behavior in these animals (8). To determine whether the increase in adiposity observed in IL-18R$^{-/-}$ mice was attributable to an increase in food intake or a decrease in energy expenditure (or both), we next performed whole-body indirect calorimetry experiments. We observed no difference in food intake (Fig. 1*E*), whole-body oxygen consumption (Fig. 1*F*), or activity (data not shown) measured over 24 h when comparing IL-18R$^{-/-}$ mice with CON irrespective of diet. As expected, consumption of the HFD decreased whole-body RER, indicative of an increase in whole-body fat oxidation. When mice were provided with HFD ad libitum, average RER (over a 72-h period) was not different when comparing IL-18R$^{-/-}$ mice with CON irrespective of diet (Fig. 1*H*). Of note, however, when mice were fasted and refed at the cessation of the 72-h period, IL-18R$^{-/-}$ mice displayed a significantly higher RER in both the fasted and refed conditions, relative to CON (Fig. 1*H*).

IL-18R$^{-/-}$ mice are insulin-resistant. We next examined whether IL-18R$^{-/-}$ mice were insulin-resistant. At 3 month of age, and before the IL-18R$^{-/-}$ mice became obese on a chow diet, there were no differences in insulin resistance as measured by an intraperitoneal tolerance test (ITT) (data not shown). However, with age and irrespective of diet, IL-18R$^{-/-}$ mice displayed whole-body insulin resistance as measured by both fasting hyperinsulinemia (Fig. 2*A*) and impaired glucose clearance during an ITT (Fig. 2*B* and Supplementary Fig. 1). We next examined insulin signaling in both muscle and liver by analyzing the phosphorylation of Akt (Ser^{473}) before and 2 min after a bolus dose of insulin. Although insulin increased pAkt in the skeletal muscle (Fig. 2*C*) and liver (Fig. 2*E*) of CON animals fed a chow diet, this effect was markedly blunted in IL-18R$^{-/-}$ mice (Fig. 2*C* and *E*). No differences in pAkt in either skeletal muscle (Fig. 2*D*) or liver (Fig. 2*F*) were observed when comparing IL-18R$^{-/-}$ with CON mice when fed an HFD.

IL-18R$^{-/-}$ mice store excess lipid in skeletal muscle and have inflamed livers and skeletal muscle. Excess adiposity often is associated with ectopic lipid storage in metabolic tissues such as liver and skeletal muscle, which can mediate insulin resistance either directly or via the upregulation of serine threonine kinases such as c-jun terminal kinase (JNK) and inhibitor of κB kinase (5). Accordingly, we next measured intramyocellular and intrahepatic lipid content and the phosphorylation of JNK (Thr^{183}/Tyr^{185}) and inhibitor of κB kinase-αβ (Ser^{180}/ Ser^{181}) in these tissues. Irrespective of diet, triacylglycerol content was higher in the skeletal muscles of IL-18R$^{-/-}$ relative to CON mice (Fig. 3*A*). This was associated with elevated JNK (Fig. 3*B*) but not with inhibitor of κB-kinase (Supplementary Fig. 2) phosphorylation. Conversely, we did not observe any differences in intrahepatic triacylglycerol concentration when comparing IL-18R$^{-/-}$ with CON mice irrespective of diet (Fig. 3*C*). Notwithstanding, phosphorylation of JNK (Fig. 3*D*) and the mRNA expression of key fatty acid synthesis transcription factors/enzyme sterol regulatory–element binding protein-1c and *FAS* (Fig. 3*E* and *F*) were elevated in the liver when comparing IL-18R$^{-/-}$ with CON mice when animals were fed a chow and an HFD. However, no differences were observed in the mRNA expression of key gluconeogenic enzymes *PEPCK* or glucose-6 phosphate dehydrogenase when comparing IL-18R$^{-/-}$ with CON mice irrespective of diet (Supplementary Fig. 3). Given that neither hepatosteatosis nor the expression of key enzymes involved in regulating hepatic glucose production was different when comparing IL-18R$^{-/-}$ with CON mice, it is unlikely that changes in liver insulin sensitivity were responsible for the reduced whole-body insulin sensitivity observed in IL-18R$^{-/-}$, although this possibility cannot be entirely ruled out.

IL-18R$^{-/-}$ mice have reduced AMPK signaling in metabolic tissues. Because IL-18R$^{-/-}$ mice are prone to weight gain on a normal diet and ectopic lipid storage independent of feeding, we next examined whether pathways associated with lipid oxidation were impaired. One major pathway that regulates fatty acid oxidation is AMPK. AMPK phosphorylates ACCβ, resulting in inhibition of ACC activity, which in turn leads to a decrease in malonyl CoA content, relieving inhibition of CPT1 and increasing fatty acid oxidation. No significant differences between phenotypes were observed when measuring the phosphorylation of AMPK (Thr^{172}) (data not shown). However, the phosphorylation of ACCβ (Ser^{218}), a downstream marker of AMPK activity, was reduced in the skeletal muscle, liver, and adipose tissue of IL-18R$^{-/-}$ when fed a chow diet (Fig. 4*A–C*). In addition, this effect was maintained in skeletal muscle (Fig. 4*A*) and liver (Fig. 4*B*), but not adipose tissue (Fig. 4*C*) when mice were fed the HFD.

Exogenous IL-18 treatment increases AMPK signaling and fat oxidation in skeletal muscle in vitro and ex vivo. Because we observed that IL-18R$^{-/-}$ mice become obese, store more lipid in skeletal muscle, and have defective ACCβ phosphorylation in this organ, we next performed in vitro and ex vivo experiments in muscle cells and whole muscle strips to confirm the role of IL-18 on AMPK signaling and fat oxidation in this important metabolic tissue. In initial experiments, we demonstrated that as little as 1.0 ng/mL recombinant IL-18 protein was sufficient to phosphorylate both AMPK (Thr^{172}) (Fig. 5*A*) and ACCβ (Ser^{218}) (Fig. 5*B*) in L6 myotubes. We next performed experiments in isolated intact soleus muscle as previously reported (16,20,21). Treating these muscles with 100 ng/mL recombinant IL-18 was sufficient to increase both palmitate oxidation (Fig. 5*C*) and AMPK phosphorylation (Thr^{172}) (Fig. 5*D*).

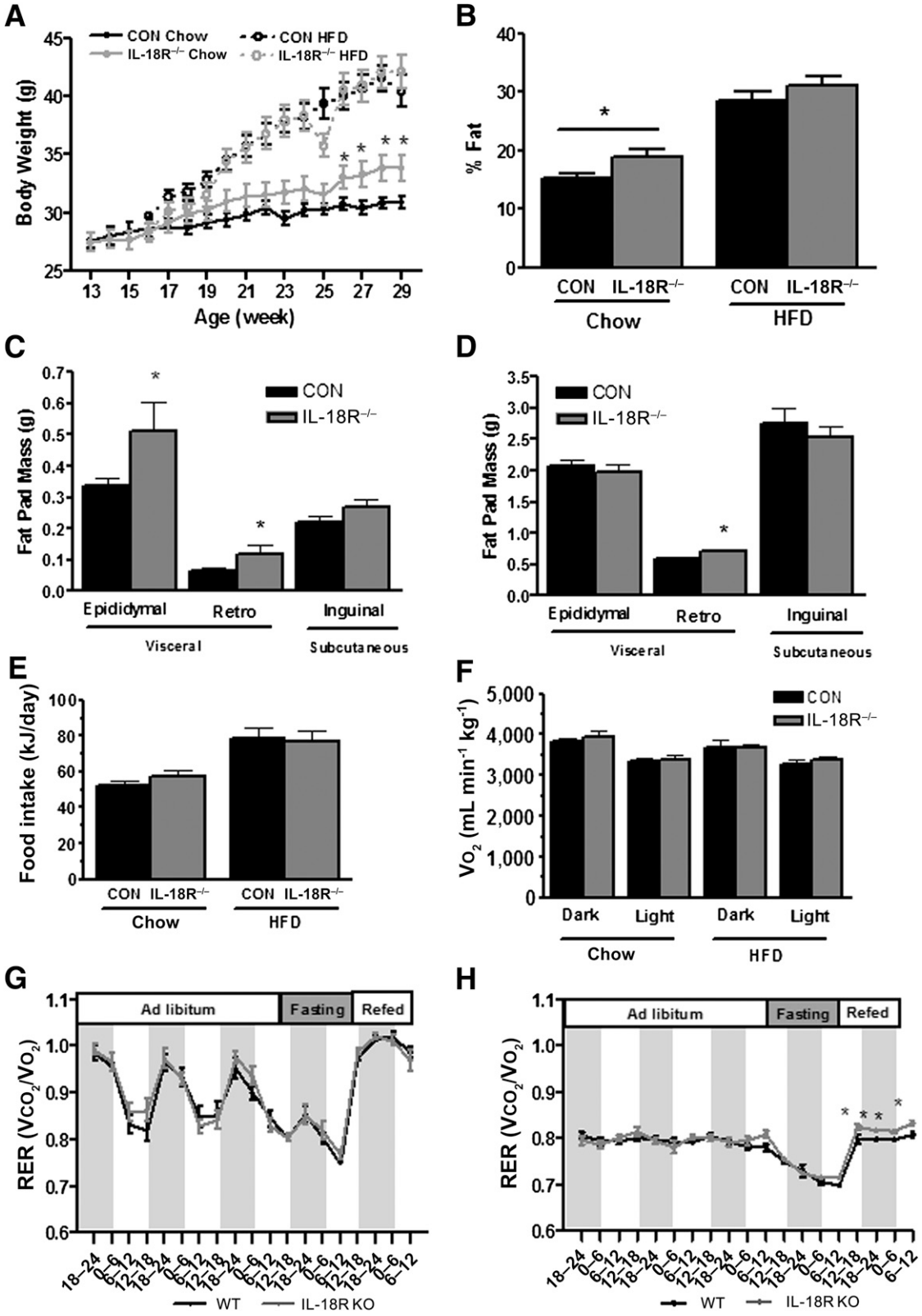

FIG. 1. Whole-body phenotype of IL-18R$^{-/-}$ mice. *A*: Growth curves during chow and HFD (CON-chow: n = 21; CON-HFD: n = 12; IL-18R$^{-/-}$-chow: n = 14; IL-18R$^{-/-}$-HFD: n = 14). *B*: Fat percentage during chow and HFD (CON-chow: n = 19; CON-HFD: n = 19; IL-18R$^{-/-}$-chow: n = 12; IL-18R$^{-/-}$-HFD: n = 11). *C*: Inguinal, gonadal, and retroperitoneal fat pads during chow diet (CON = 13; IL-18R$^{-/-}$: n = 7). *D*: Inguinal, gonadal, and retroperitoneal fat pads during HFD (CON = 11; IL-18R$^{-/-}$: n = 10). Average 24-h food intake (*E*) and Vo_2 (*F*) during 2 days of chow and HFD and RER during 3 days of ad libitum feeding, 24-h fasting, and 24-h refeeding of chow (*G*) and HFD (*F*) obtained from control (black bars) and IL-18R$^{-/-}$ (gray bars) male mice at 7 months of age mice (CON-chow: n = 7; CON-HFD: n = 8; IL-18R$^{-/-}$-chow: n = 8; IL-18R$^{-/-}$-HFD: n = 6). Results are presented as mean ± SEM. *P < 0.05 vs. controls. CON, control; KO, knockout; Retro, retroperitoneal; WT, wild-type.

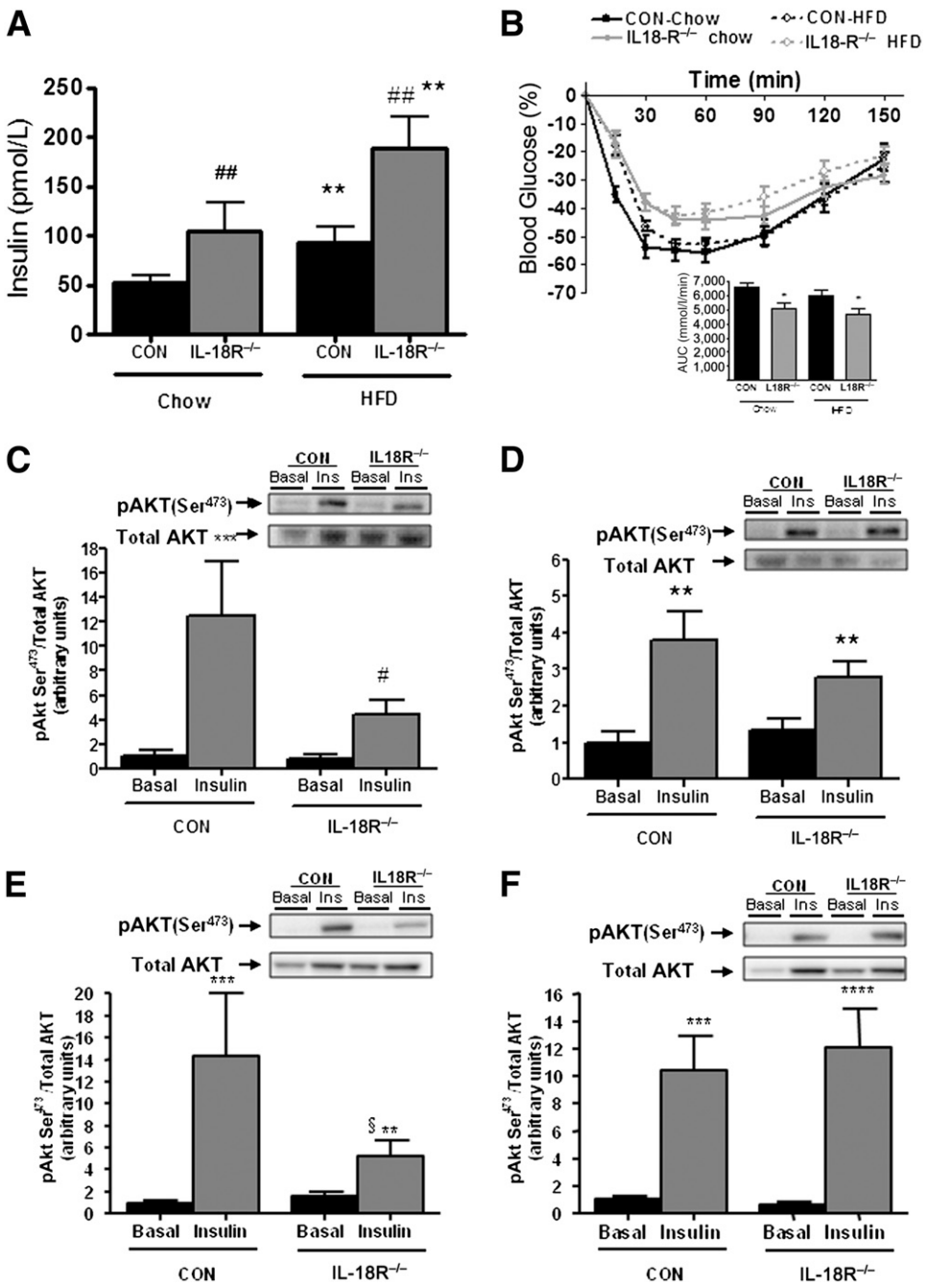

FIG. 2. IL-18R$^{-/-}$ mice exhibit insulin resistance when fed a chow diet and an HFD. *A*: Plasma insulin (CON-chow: $n = 7$; CON-HFD: $n = 8$; IL-18R$^{-/-}$ -chow: $n = 8$; IL-18R$^{-/-}$ -HFD: $n = 6$). *B*: Insulin tolerance with area under the curve (AUC) inserted (CON-chow: $n = 12$; CON-HFD: $n = 12$; IL-18R$^{-/-}$ -chow: $n = 14$; IL-18R$^{-/-}$ -HFD: $n = 12$) For the actual data, see Supplementary Fig. 1. Total and phosphorylated Ser^{473} during chow diet (*C*; $n = 4$–6) and HFD (*D*) ($n = 8$–9) in muscle and total and phosphorylated Ser^{473} during chow diet (*E*; $n = 5$–6) and HFD (*F*; $n = 7$–9) in liver. Total Akt was performed separately and was not stripped. The signaling data were obtained in littermate controls. Samples from chow diet and HFD were run on separate gels. Results are presented as mean ± SEM . *$P < 0.05$; **$P < 0.01$, ***$P < 0.001$ vs. chow (*A*) or vs. basal (*C–F*). #$P < 0.05$; ##$P < 0.01$ vs. control (*A*, *C*). §Interaction between genotype and diet $P = 0.06$ (*E*). CON, control; Ins, insulin; pAkt, phosphorylated Akt.

Ectopic expression of IL-18 in a single tibialis anterior muscle is sufficient to protect against excess adipose tissue storage in mice fed an HFD. To determine whether the results obtained in muscle cell and ex vivo muscle strips also were prevalent in vivo, we used the in vivo electroporation technique to overexpress *IL-18* cDNA in the tibialis anterior muscles of C57BL/6J mice that were placed on an HFD diet for 4 weeks. Using this technique, we previously have observed a transfection efficiency of ~60%, as measured by the electroporation of a GFP construct as a control (21). IL-18 protein expression in the tibialis anterior was increased 30- to 40-fold above basal when compared with mice when the tibialis anterior was electroporated with an empty vector (sham) (Fig. 6*A*). No difference in body weight was observed when comparing IL-18 with sham electroporated mice (Fig. 6*B*). In accordance with this observation, adiposity was reduced when comparing IL-18 with sham electroporated mice at 4 weeks (Fig. 6*C* and *D* and Supplementary Fig. 4). However, this reduction in adiposity was insufficient to result

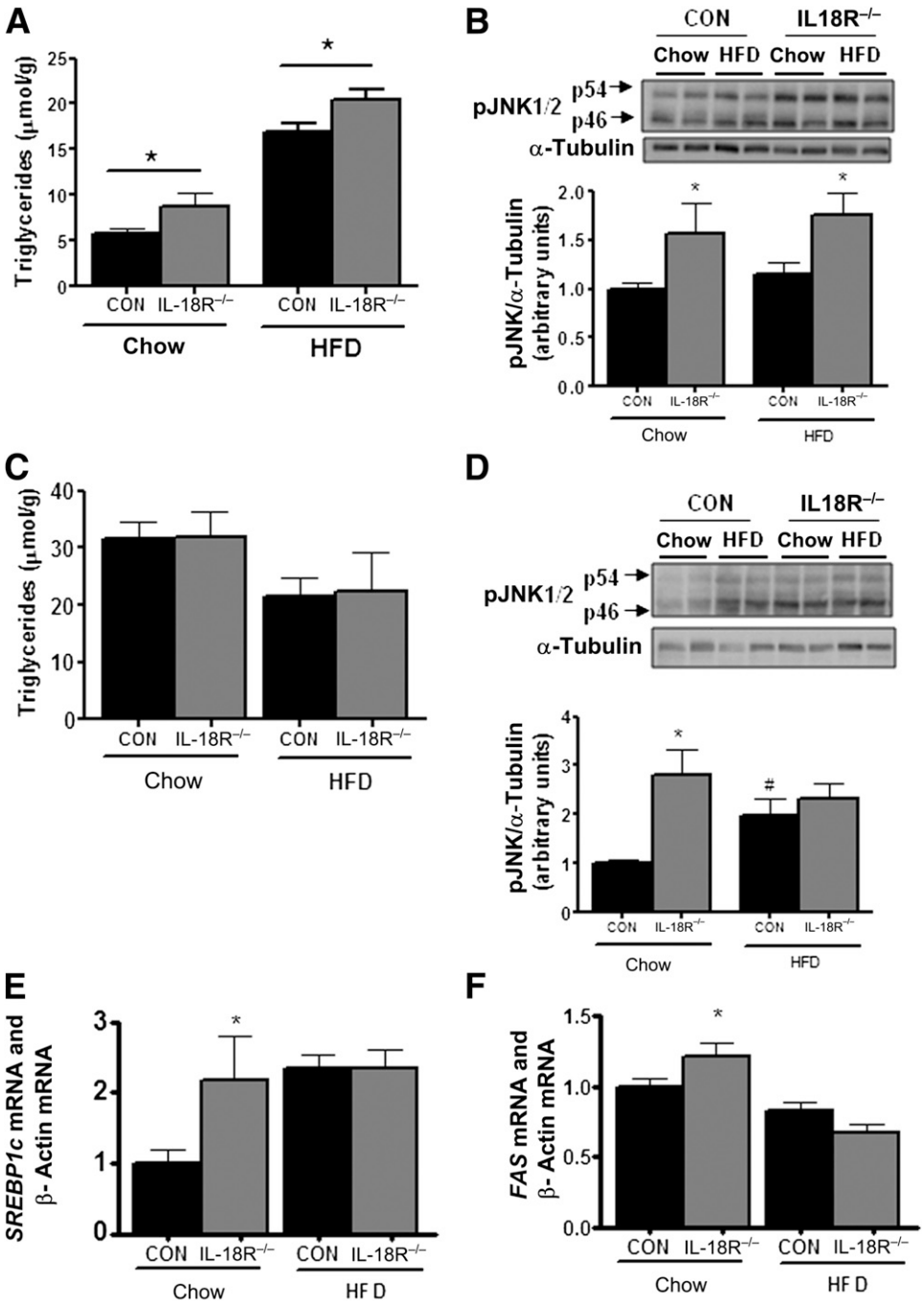

FIG. 3. IL-18R$^{-/-}$ mice develop hyperlipidemia and inflammation on a chow diet but not on an HFD. *A*: Triglycerides in muscle (CON-chow: n = 17; CON-HFD: n = 9; IL-18R$^{-/-}$-chow: n = 8; IL-18R$^{-/-}$-HFD: n = 5). *B*: Representative immunoblot and densitometric quantification of JNK1/2 phosphorylation in soleus muscle (n = 7–8). *C*: Triglycerides in liver (n = 5–8). *D*: Representative immunoblot and densitometric quantification of JNK1/2 phosphorylation in liver (n = 6–8). mRNA levels of *SREBP1c* (*E*) in liver (n = 9–19) and mRNA levels of *FAS* (*F*) in liver (n = 9–19) during chow and HFD obtained from control (black bars) and IL-18R$^{-/-}$ (gray bars) male mice at 7 months of age. Results are presented as mean ± SEM. *P < 0.05 vs. control. #P < 0.05 vs. chow diet. CON, control; pJNK, phosphorylated JNK; *SREBP1c*, sterol regulatory–element binding protein-1c.

in increased whole-body insulin sensitivity or glucose tolerance as measured by ITT and glucose tolerance test (Supplementary Fig. 5).

Ectopic expression of IL-18 in a single tibialis anterior muscle increases AMPK signaling and markers of lipid oxidation in this organ. We next measured AMPK signaling and markers of lipid oxidation in IL-18 and sham electroporated muscles. Both AMPK activity (Fig. 7*A*) and ACCβ phosphorylation (Ser^{218}) (Fig. 7*B*) were markedly elevated in IL-18 compared with sham electroporated muscles. In addition, we also observed increased mRNA abundance of β-hydroxyacyl-CoA-dehydrogenase, a key enzyme involved in mitochondrial function (Fig. 7*C*) and *CPT1* (Fig. 7*D*), the enzyme that controls the transfer of long-chain fatty acyl CoA into mitochondria and enhances rates of fatty acid oxidation in the IL-18 electroporated mice relative to sham mice. It is now well-known that skeletal muscle can act as an endocrine organ, producing "myokines" to result in tissue cross-talk (22). To examine whether IL-18 could act as

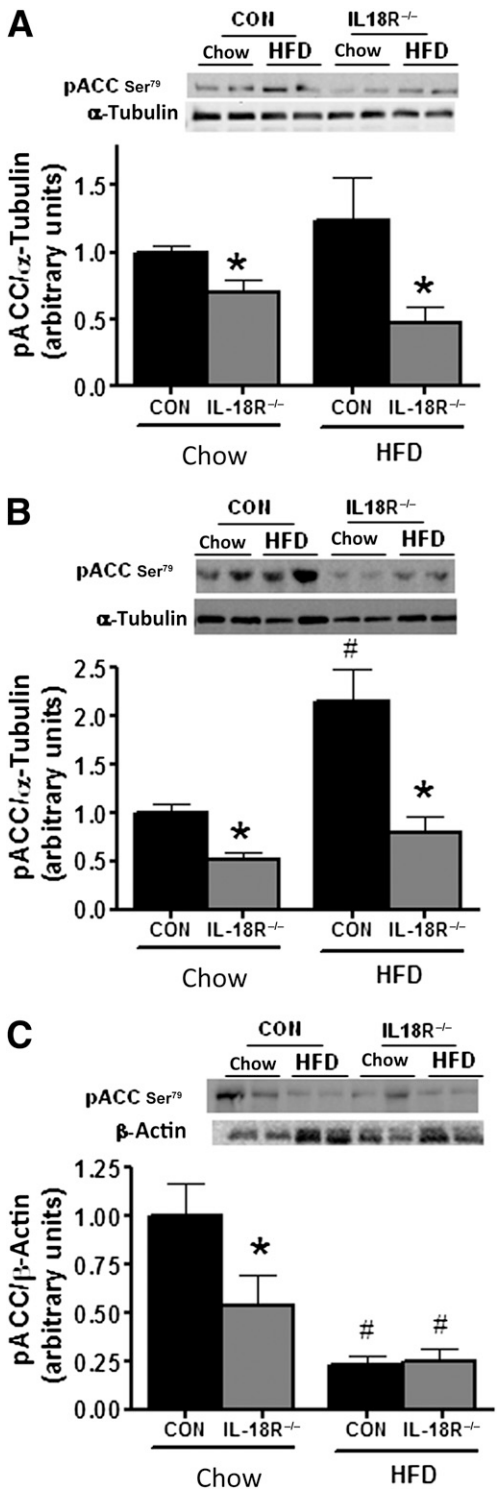

FIG. 4. IL-18R$^{-/-}$ mice exhibit blunted phosphorylation of ACCβ in muscle, liver, and adipose tissue. Representative immunoblot and densitometric quantification (*A*) of ACCβ phosphorylation in soleus muscle (n = 7–8), representative immunoblot and densitometric quantification (*B*) of ACCβ phosphorylation in liver (n = 5–8), and representative immunoblot and densitometric quantification (*C*) of ACCβ phosphorylation in adipose tissue (n = 6–10) during chow and HFD obtained from control (black bars) and IL-18R$^{-/-}$ (gray bars) male mice at 7 months of age. Results are presented as mean ± SEM. *P < 0.05 vs. control; #P < 0.05 vs. chow diet. CON, control; pACC, phosphorylated ACC.

a myokine when overexpressed in skeletal muscle, we examined circulating levels of IL-18 and markers of insulin sensitivity, fat oxidation, and inflammation in other tissues such as the liver and adipose. Despite the increase in intramuscular IL-18 expression with electroporation, plasma IL-18 was not elevated in the IL-18 electroporated mice relative to sham (Supplementary Fig. 5). Therefore, it was not surprising that pAkt, pAMPK, pACC, and pJNK were not altered in the liver or adipose tissue of IL-18 electroporated mice relative to sham mice (Supplementary Figs. 5 and 6). Together, these data provide evidence that IL-18 can activate AMPK in skeletal muscle in vivo.

DISCUSSION

IL-18 signaling has been implicated in the etiology of metabolic homeostasis and insulin resistance; however, studies in IL-18–deficient mice have suggested that IL-18 is required to prevent hyperphagia (8,9). In the current study, rather than use a model of genetic deletion of IL-18, we initially studied mice that harbor a global deletion of the functional IL-18R. We show that IL-18R$^{-/-}$ mice are prone to weight gain on a chow diet and develop insulin resistance, a phenotype that is associated with ectopic skeletal muscle lipid expression, inflammation, and reduced AMPK signaling.

The IL-18R$^{-/-}$ mice displayed significantly increased body weight and increased fat pad mass after ~26 weeks of age. Although others have shown that IL-18–deficient mice display hyperphagia (8,9), we did not observe this in the IL-18R$^{-/-}$ mice. We were careful to monitor food intake in their normal habitat and during metabolic caging, so we are confident that the food intake between the IL-18R$^{-/-}$ and CON mice were comparable. Given the identical oxygen consumption between the IL-18R$^{-/-}$ and CON mice, why would the IL-18R$^{-/-}$ mice gain more weight if both energy input and expenditure were comparable? It should be noted that the difference in body weight when comparing the IL-18R$^{-/-}$ and CON mice was ~10% by the end of the study (Fig. 1*A*), whereas the overall difference in percent body fat was ~4% (Fig. 1*B*). This would equate to an approximate increase of 0.15 g fat or 0.70 kJ energy per day. The daily energy expenditure of a mouse has been estimated to be 42 kJ per day (23). Consequently, <2% difference in daily energy expenditure would be sufficient to result in the increased body weight but was unlikely to be detected with available techniques, such as metabolic caging. Similar problems have been encountered in other mouse models of obesity (23,24), and work from our group also has recently observed such an anomaly (25). Notwithstanding this apparent anomaly, it appears, based on the data we have reported, that the IL-18R$^{-/-}$ mice gain weight and store excess lipid in skeletal muscle, which results in whole-body and skeletal muscle insulin resistance.

It has been suggested that IL-18R also might be activated by ligands other than IL-18 (26,27), and this, potentially, could explain why hyperphagia previously was observed in IL-18–deficient mice (8,9) but not in IL-18R$^{-/-}$ mice in the current study. Interestingly, when mice fed an HFD were fasted and refed, IL-18R$^{-/-}$ mice displayed a significantly higher RER in the refed condition (Fig. 1*H*). This suggests that mice lacking the IL-18R cannot oxidize lipids and rely on utilization of carbohydrates as a preferred energy substrate during refeeding. This is supported by our gain-of-function data (IL-18 increased fat oxidation). Interestingly, Zorrilla et al. (9) observed that mice with

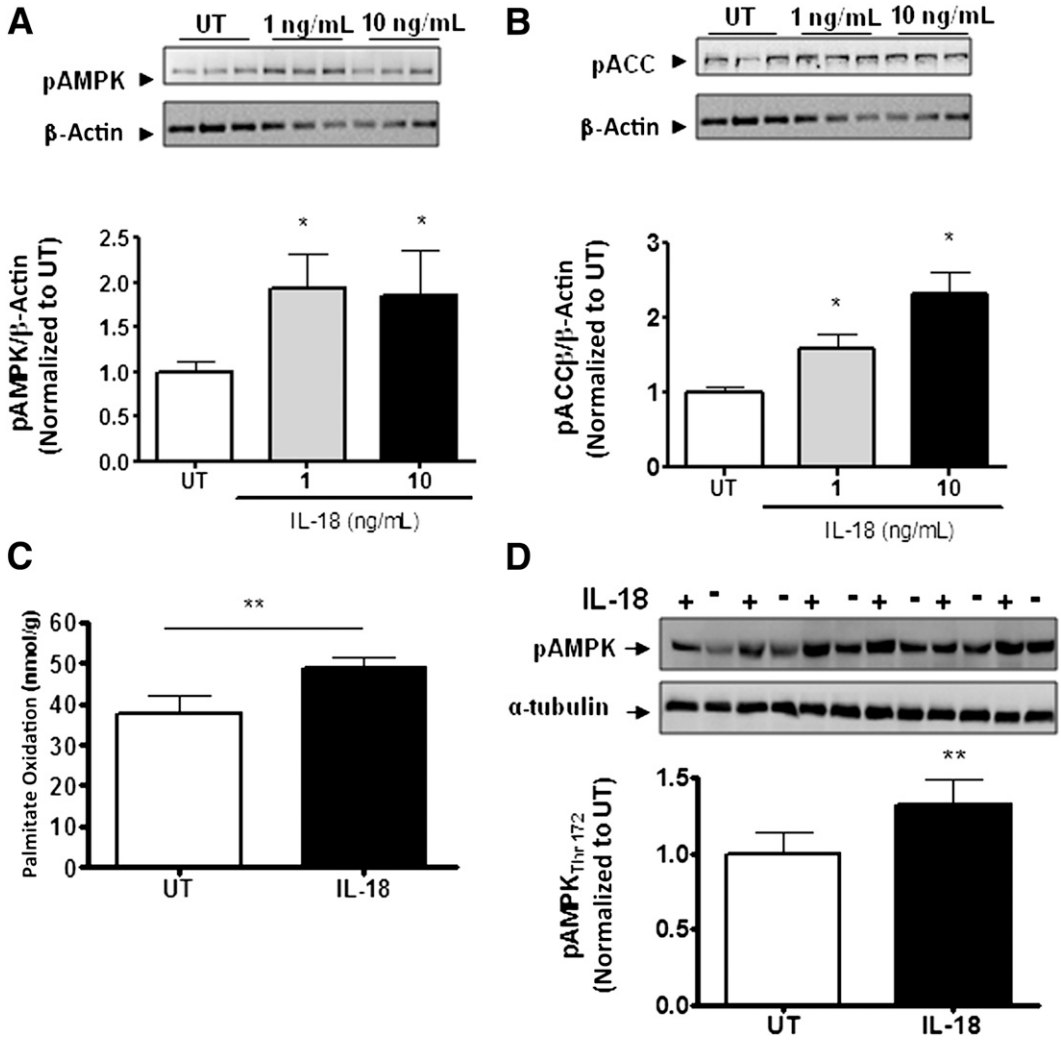

FIG. 5. IL-18 increases fatty acid oxidation and AMPK signaling in skeletal muscle in vitro and ex vivo. Representative immunoblot and densitometric quantification of AMPK Thr^{172} in L6 cells (*A*) stimulated with 1 ng/mL and 10 ng/mL IL-18 for 30 min (n = 9/dose), representative immunoblot and densitometric quantification of ACCβ phosphorylation in L6 cells (*B*) stimulated with 1 ng/mL and 10 ng/mL IL-18 for 30 min (n = 9/dose), fatty acid oxidation (*C*) in isolated soleus muscle strips in the presence of IL-18 (100 ng/mL) or PBS (untreated [UT]) (n = 10/group), and representative immunoblot and densitometric quantification (*D*) of AMPK Thr^{172} phosphorylation in isolated soleus muscle strips in the presence of IL-18 (100 ng/mL) or PBS (UT) (n = 6/group). Results are presented as mean ± SEM. *P < 0.05; **P < 0.01 vs. control (UT). pACC, phosphorylated ACC; pAMPK, phosphorylated AMPK.

IL-18 deficiency were not hyperphagic when fed an HFD and suggested that they differentially process carbohydrate-rich compared with lipid-rich diets or differentially use these macronutrients as fuel. Our study supports this hypothesis.

By performing whole-body insulin tolerance tests, we cannot ascertain whether the whole-body insulin resistance observed in the IL-18R$^{-/-}$ mice relative to control mice was attributable to insulin resistance in skeletal muscle, liver, or a combination of the two. However, several lines of evidence suggest that the defect in the IL-18R$^{-/-}$ mice was primarily in the skeletal muscle, and this is the rationale for choosing to study this organ in depth. First, it is well-acknowledged that ectopic lipid expression is a primary mechanism leading to insulin resistance (28). Whereas intramuscular triglycerides were elevated in the IL-18R$^{-/-}$ mice relative to CON mice, no such increase was observed in the liver (Fig. 3). Second, the mRNA expression of key gluconeogenic enzymes PEPCK and glucose-6 phosphate dehydrogenase were not different in the liver of the IL-18R$^{-/-}$ mice. Third, even though the IL-18R$^{-/-}$ mice were insulin-resistant on an HFD relative to CON mice, there was no evidence of decreased pAkt (Fig. 2*F*) or of mRNA expression of *SREBP1* or *FAS* (Fig. 3*E* and *F*) in the liver. Together, these data suggest that skeletal muscle was the origin of the primary defect, although we acknowledge that the effects of IL-18R$^{-/-}$ on the liver cannot be completely discounted because we did not directly measure insulin sensitivity in this organ.

Of note was our observation that pJNK was markedly elevated in the livers of the IL-18R$^{-/-}$ mice relative to CON mice despite equivalent lipid content when animals were fed a chow diet (Fig. 3). Although this may seem counterintuitive, this observation is not novel. We previously have observed such a phenomenon in IL-6–deficient mice (25). A potential mechanism recently has been proposed by Flavell et al., who demonstrated that NLRP6 and NLRP3 inflammasomes and, importantly, IL-18 negatively regulates nonalcoholic fatty liver disease/nonalcoholic steatohepatitis progression as well as multiple aspects of

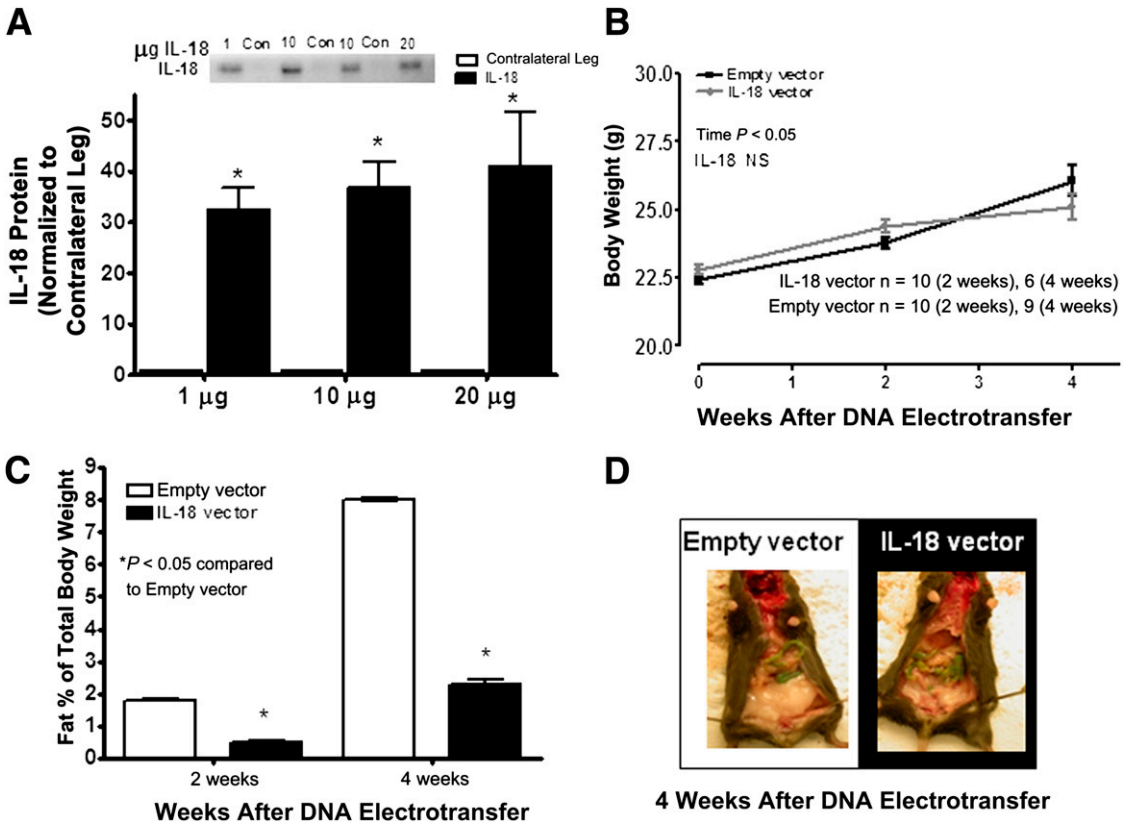

FIG. 6. Mice overexpressing IL-18 in skeletal muscle are protected from diet-induced obesity. Densitometric quantification of IL-18 protein (*A*) in the tibialis anterior muscle after DNA electrotransfer of 1 μg, 10 μg, and 20 μg plasmid (n = 6/dose), growth curves (*B*; n = 6–10), fat percentage (*C*; n = 6–10), and image of mice overexpressing IL-18 (*D*) in the tibialis anterior muscle (filled bars) after 4 weeks of an HFD compared with mice overexpressing an empty vector (open bars). Results are presented as mean ± SEM. *P < 0.05 vs. empty vector. Con, control; NS, not significant.

metabolic syndrome via modulation of the gut microbiota not necessarily related to hepatosteatosis (29). Although speculative, the increased inflammation observed in the IL-18R$^{-/-}$ mice in the presence of relatively normal lipid levels may be related to such a mechanism.

Based on our loss-of-function and gain-of-function models, IL-18 signaling is implicated in fatty acid oxidation rates in skeletal muscle as a result of activation of AMPK. As discussed, AMPK phosphorylates ACCβ, resulting in inhibition of ACC activity, which in turn leads to a decrease in malonyl CoA content, relieving inhibition of CPT1 and increasing fatty acid oxidation. The phosphorylation of ACCβ was reduced in the skeletal muscle, liver, and adipose tissue of IL-18R$^{-/-}$ (Fig. 4). Moreover, when cultured skeletal muscle cells or isolated skeletal muscle strips were treated with IL-18, phosphorylation of AMPK or ACC (or both) was increased and, in the case of intact ex vivo–treated skeletal muscle, this increase was associated with enhanced fatty acid oxidation. Finally, when IL-18 was overexpressed in skeletal muscle in vivo, AMPK activity and ACC phosphorylation were increased, not only in the electoporated muscle (Fig. 7*A* and *B*). Taken together, the data provide evidence implicating IL-18 in the activation of AMPK.

It is now well-known that many cytokines, including leptin, adiponectin, ghrelin, IL-6, and ciliary neurotrophic factor can activate AMPK (30,31), but this is the first report indicating that IL-18 can act as an AMPK agonist. This observation, however, is consistent with these previous studies because IL-18 can act as an activator of STAT3 (4). Work from our group previously has shown that members of the IL-6 family of cytokines, which potently activate STAT3, also enhance fat oxidation via AMPK (11,12). Importantly, when mice that harbor a truncation of the COOH-terminal domain that eliminates these tyrosine residues on the gp130 receptor (gp130$^{\Delta STAT}$ mice) are treated with CNTF, the phosphorylation of STAT3 is abolished, as is the activation of AMPK (12).

Although feeding mice an HFD did not result in differences in body weight, fat mass, or insulin signaling in skeletal muscle and liver when comparing the genotypes, the IL-18R$^{-/-}$ mice nevertheless displayed elevated fasting insulin levels and impaired insulin tolerance as measured by an ITT (Fig. 2). Although speculative, this may be attributable to the fact that under HFD conditions, the activation of the AMPK pathway remained impaired in the IL-18R$^{-/-}$ mice, at least in skeletal muscle and liver (Fig. 4), leading to elevated lipid levels in skeletal muscle of the IL-18R$^{-/-}$ mice under HFD conditions (Fig. 3).

In summary, we have identified that IL-18 can activate AMPK. Moreover, mice that harbor a genetic deletion of a functional IL-18R are prone to weight gain and development of insulin resistance and inflammation in important metabolic tissues such as skeletal muscle and liver. Therefore, our data add IL-18 to a growing list of catabolic proinflammatory cytokines that paradoxically are required to maintain pathways important for fatty acid oxidation and thus prevent insulin resistance.

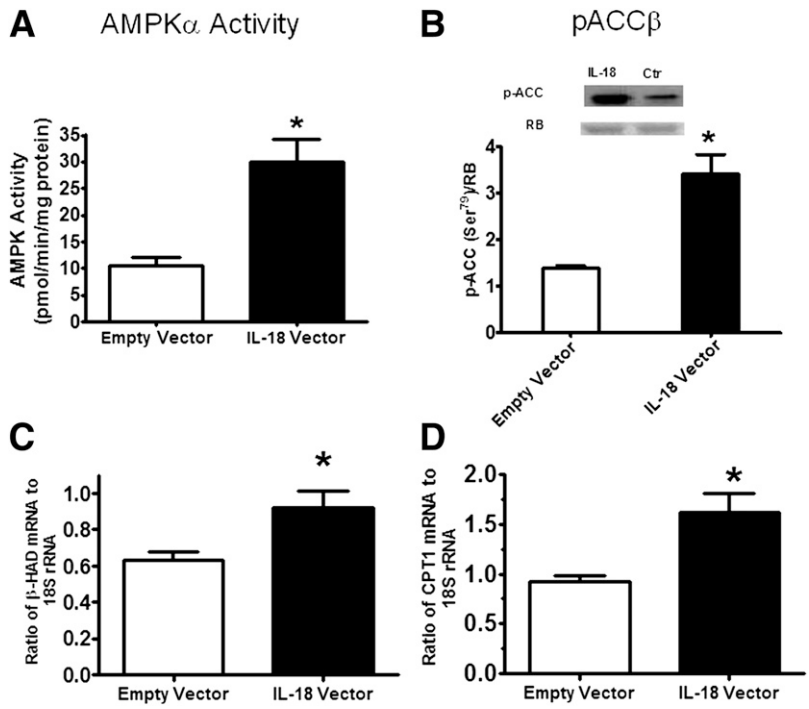

FIG. 7. Mice overexpressing IL-18 in skeletal muscle have enhanced AMPK signaling. AMPKα1 (*A*) activity (n = 6/group), representative immunoblot and densitometric quantification of ACCβ (*B*) phosphorylation (n = 6/group), mRNA levels (*C*) of β-hydroxyacyl-CoA-dehydrogenase (*β-HAD*) (n = 8/group), and mRNA levels (*D*) of *CPT1β* (n = 7/group) in the muscle overexpressing IL-18 (filled bars) compared with a muscle electroporated with an empty vector (open bars). Results are presented as mean ± SEM. *$P < 0.05$ vs. empty vector. pACC, phosphorylated ACC; RB, reactive brown was used as loading control; Ctr, control.

ACKNOWLEDGMENTS

This study was supported, in part, by a grant from the National Health and Medical Research Council of Australia (NHMRC grant no. 526606). This study was further supported by the Danish Council for Independent Research–Medical Sciences, the Commission of the European Communities (grant agreement no. 223576-MYOAGE), and by grants from the Novo Nordisk Foundation, Hørslevfonden, the Danish National Research Foundation (#10-083807), Højmosegårdlegatet, Fonden for Lægevidenskabens Fremme, and Direktør Jacob Madsen og Hustru Olga Madsens Fond. The Centre of Inflammation and Metabolism (CIM) and The Rodent Metabolic Phenotyping Center is part of the UNIK Project: Food, Fitness & Pharma for Health and Disease (see www.foodfitnesspharma.ku.dk) supported by the Danish Ministry of Science, Technology, and Innovation. The CIM is a member of DD2-the Danish Center for Strategic Research in Type 2 Diabetes (the Danish Council for Strategic Research, grant no. 09-067009 and 09-075724). The Copenhagen Muscle Research Centre is supported by a grant from the Capital Region of Denmark. M.A.F. is a Senior Principal Research Fellow, M.J.W. is a Senior Research Fellow, and C.R.B. and V.B.M. are Career Development Fellows of the NHMRC. The CIM is supported by a grant from the Danish National Research Foundation (#02-512-55). B.L. was supported by a grant from the Danish National Research Foundation (#09-063656). B.L. received postdoctoral fellowship support from a grant from the Danish National Research Foundation.

No other potential conflicts of interest relevant to this article were reported.

B.L. designed research, performed and/or analyzed research, and wrote the manuscript. V.B.M., C.B., P.H., T.L.A., E.E., M.J.W., C.R.B., O.H.M., S.S., C.R., J.A., H.P., S.D., T.J.A., and A.N.M. performed and/or analyzed research. J.H. contributed new reagents and analytical tools. B.K.P. designed research. M.A.F. designed research and wrote the manuscript. All authors contributed to the writing of the final submitted version of the manuscript. B.L. is the guarantor of this work and, as such, had full access to all of the data in the study and takes responsibility for the integrity of the data and the accuracy of the data analysis.

The authors acknowledge the assistance of Betina Mentz, Ruth Rousing, Hanne Villumsen, Lone Nielsen, Andreas Nygaard Madsen (University of Copenhagen), Steve Risis (Baker IDI Heart and Diabetes Institute), and the Rodent Metabolic Phenotyping Center (University of Copenhagen).

REFERENCES

1. Okamura H, Tsutsi H, Komatsu T, et al. Cloning of a new cytokine that induces IFN-gamma production by T cells. Nature 1995;378:88–91
2. Alboni S, Cervia D, Sugama S, Conti B. Interleukin 18 in the CNS. J Neuroinflammation 2010;7:9
3. Shapiro L, Puren AJ, Barton HA, et al. Interleukin 18 stimulates HIV type 1 in monocytic cells. Proc Natl Acad Sci USA 1998;95:12550–12555
4. Chandrasekar B, Patel DN, Mummidi S, Kim JW, Clark RA, Valente AJ. Interleukin-18 suppresses adiponectin expression in 3T3-L1 adipocytes via a novel signal transduction pathway involving ERK1/2-dependent NFATc4 phosphorylation. J Biol Chem 2008;283:4200–4209
5. Hotamisligil GS. Inflammation and metabolic disorders. Nature 2006;444:860–867
6. Esposito K, Pontillo A, Ciotola M, et al. Weight loss reduces interleukin-18 levels in obese women. J Clin Endocrinol Metab 2002;87:3864–3866
7. Aso Y, Okumura K, Takebayashi K, Wakabayashi S, Inukai T. Relationships of plasma interleukin-18 concentrations to hyperhomocysteinemia and carotid intimal-media wall thickness in patients with type 2 diabetes. Diabetes Care 2003;26:2622–2627
8. Netea MG, Joosten LA, Lewis E, et al. Deficiency of interleukin-18 in mice leads to hyperphagia, obesity and insulin resistance. Nat Med 2006;12:650–656

9. Zorrilla EP, Sanchez-Alavez M, Sugama S, et al. Interleukin-18 controls energy homeostasis by suppressing appetite and feed efficiency. Proc Natl Acad Sci USA 2007;104:11097–11102
10. Inoue H, Ogawa W, Ozaki M, et al. Role of STAT-3 in regulation of hepatic gluconeogenic genes and carbohydrate metabolism in vivo. Nat Med 2004; 10:168–174
11. Carey AL, Steinberg GR, Macaulay SL, et al. Interleukin-6 increases insulin-stimulated glucose disposal in humans and glucose uptake and fatty acid oxidation in vitro via AMP-activated protein kinase. Diabetes 2006;55: 2688–2697
12. Watt MJ, Dzamko N, Thomas WG, et al. CNTF reverses obesity-induced insulin resistance by activating skeletal muscle AMPK. Nat Med 2006;12: 541–548
13. Minokoshi Y, Kim YB, Peroni OD, et al. Leptin stimulates fatty-acid oxidation by activating AMP-activated protein kinase. Nature 2002;415:339–343
14. Al-Khalili L, Bouzakri K, Glund S, Lönnqvist F, Koistinen HA, Krook A. Signaling specificity of interleukin-6 action on glucose and lipid metabolism in skeletal muscle. Mol Endocrinol 2006;20:3364–3375
15. Febbraio MA. gp130 receptor ligands as potential therapeutic targets for obesity. J Clin Invest 2007;117:841–849
16. Matthews VB, Aström MB, Chan MH, et al. Brain-derived neurotrophic factor is produced by skeletal muscle cells in response to contraction and enhances fat oxidation via activation of AMP-activated protein kinase. Diabetologia 2009;52:1409–1418
17. Hojman P, Gissel H, Andre FM, et al. Physiological effects of high- and low-voltage pulse combinations for gene electrotransfer in muscle. Hum Gene Ther 2008;19:1249–1260
18. Hojman P, Eriksen J, Gehl J. Tet-On induction with doxycycline after gene transfer in mice: sweetening of drinking water is not a good idea. Anim Biotechnol 2007;18:183–188
19. Bruce CR, Dyck DJ. Cytokine regulation of skeletal muscle fatty acid metabolism: effect of interleukin-6 and tumor necrosis factor-alpha. Am J Physiol Endocrinol Metab 2004;287:E616–E621
20. Bruce CR, Hoy AJ, Turner N, et al. Overexpression of carnitine palmitoyltransferase-1 in skeletal muscle is sufficient to enhance fatty acid oxidation and improve high-fat diet-induced insulin resistance. Diabetes 2009;58:550–558
21. Henstridge DC, Bruce CR, Pang CP, et al. Skeletal muscle-specific overproduction of constitutively activated c-Jun N-terminal kinase (JNK) induces insulin resistance in mice. Diabetologia 2012;55:2769–2778
22. Pedersen BK, Febbraio MA. Muscle as an endocrine organ: focus on muscle-derived interleukin-6. Physiol Rev 2008;88:1379–1406
23. Tschöp M, Smiley DL, Heiman ML. Ghrelin induces adiposity in rodents. Nature 2000;407:908–913
24. García MC, Wernstedt I, Berndtsson A, et al. Mature-onset obesity in interleukin-1 receptor I knockout mice. Diabetes 2006;55:1205–1213
25. Matthews VB, Allen TL, Risis S, et al. Interleukin-6-deficient mice develop hepatic inflammation and systemic insulin resistance. Diabetologia 2010; 53:2431–2441
26. Lewis EC, Dinarello CA. Responses of IL-18- and IL-18 receptor-deficient pancreatic islets with convergence of positive and negative signals for the IL-18 receptor. Proc Natl Acad Sci USA 2006;103:16852–16857
27. Nold-Petry CA, Nold MF, Nielsen JW, et al. Increased cytokine production in interleukin-18 receptor alpha-deficient cells is associated with dysregulation of suppressors of cytokine signaling. J Biol Chem 2009;284:25900–25911
28. Savage DB, Petersen KF, Shulman GI. Disordered lipid metabolism and the pathogenesis of insulin resistance. Physiol Rev 2007;87:507–520
29. Henao-Mejia J, Elinav E, Jin C, et al. Inflammasome-mediated dysbiosis regulates progression of NAFLD and obesity. Nature 2012;482:179–185
30. Hardie DG. AMP-activated/SNF1 protein kinases: conserved guardians of cellular energy. Nat Rev Mol Cell Biol 2007;8:774–785
31. Ruderman NB, Keller C, Richard AM, et al. Interleukin-6 regulation of AMP-activated protein kinase. Potential role in the systemic response to exercise and prevention of the metabolic syndrome. Diabetes 2006;55 (Suppl. 2):S48–S54